Contrib Mineral Petrol (2000) 139: 720–733

Wuyi Wang · Shigeho Sueno · Eiichi Takahashi
Hisayoshi Yurimoto · Tibor Gasparik

Enrichment processes at the base of the Archean lithospheric mantle: observations from trace element characteristics of pyropic garnet inclusions in diamonds

Received: 27 April 1999 / Accepted: 1 March 2000

Abstract Trace element concentrations of peridotitic garnet inclusions in diamonds from two Chinese kimberlite pipes were determined using the ion microprobe. Garnet xenocrysts from the same two kimberlite pipes were also analyzed for comparison. In contrast to their extremely refractory major element compositions, all harzburgitic garnets showed enrichment in light rare earth elements (REE) relative to chondrite, resulting in sinuous REE patterns. Both normal and sinuous REE patterns were observed from the lherzolitic garnets. Concentrations of REE in garnets changed significantly from diamond to diamond and no specific correlations were observed with their major element compositions. Analyses of randomly selected two to three points within every grain of a large number of garnet inclusions by the ion microprobe demonstrated that there was no evident compositional heterogeneity, and multiple grains of one phase from a single diamond host also exhibit very similar compositions. This implies that the trace element heterogeneity within one grain or among multiple inclusions from the same diamond host, as reported from Siberian diamonds, is not a common feature for these Chinese diamonds. Concentrations of Na, Ti, and Zr tend to decrease when garnets become more refractory, but variations of Sr and Li are more complex. Compositions rich in light REE and relatively poor in high field strength elements (HFSE) of the harzburgitic garnet inclusions in diamonds are generally consistent with metasomatism by carbonatite melts. The trace element features observed from the garnet inclusions in Chinese diamonds may be caused by carbonatite melt infiltration and partial melt extraction. Spatial and temporal gradients in melt/rock ratio and temperature are the main reasons for the large variations of REE patterns and other trace element concentrations.

W. Wang (✉) · T. Gasparik
Center for High Pressure Research,
State University of New York, Stony Brook,
NY 11794-2100, USA
e-mail: wang@sbmp04.ess.sunysb.edu

S. Sueno
Institute of Geoscience, The University of Tsukuba,
Tennotai 1-1-1, Tsukuba, Ibaraki 305-8571, Japan

E. Takahashi · H. Yurimoto
Department of Earth and Planetary Sciences,
Tokyo Institute of Technology, Ookayama 2-12-1,
Meguro, Tokyo 152-8551, Japan

Editorial responsibility: E. H. Hauri

Introduction

Lithospheric mantle beneath the Archean cratonic areas shows some distinct features in comparison to the oceanic areas. It extends to greater depths, well into the stability field of diamond. In terms of the major element composition, it is more refractory than the oceanic lithosphere, and thus has a relatively lower density. Consequently, it has been isolated from the mantle convection for billions of years (Boyd 1989; Pearson et al. 1995a, b; Boyd et al. 1997), and thus preserved the overlying ancient crust from being destroyed. Studies of these materials from southern Africa and Siberia, transported to the earth's surface as xenoliths in kimberlites or mineral inclusions in diamonds, showed that the lithospheric mantle underneath cratons experienced complex metasomatism over a long geological period (Richardson et al. 1984; Shimizu and Richardson 1987; Shimizu et al. 1997a, b). Unlike the mantle xenoliths, which may suffer continuous interaction with the surrounding mantle, the mineral inclusions in diamonds are well protected from later chemical modifications, and thus uniquely suitable for the study of these mantle processes.

This study reports major and trace element compositions of pyropic garnet inclusions in diamonds from two Chinese kimberlite pipes. The main goals of this work have been to establish the typical concentration ranges of selected trace elements in pyropic garnet inclusions in diamonds, and to assess whether there is

any correlation between the major and trace elements. The mechanism of the enrichment process and the properties of metasomatic melts, inferred on the basis of these results, are discussed.

Samples and analysis

Mineral inclusions in diamonds studied in this report are from the "Shengli 1" and the "No.50" kimberlite pipes. These two pipes consist of typical type I kimberlite intruded into the Sino-Korea craton of northeastern China at very close geological ages (460–465 Ma). The craton consists of two major nuclei, the Liaolu terrane in the east and the Ordos terrane in the west (Fig. 1). Basement rocks of the Liaolu terrane, in which two diamondiferous kimberlite fields were found (Fuxian, Mengyin), are Archean to Early Proterozoic gneisses, with radiometric ages of 2500–3500 Ma (Jahn et al. 1987). U–Pb ages of detrital zircons indicate the existence of rocks as old as 3800 Ma (Liu et al. 1992). The geological settings of these kimberlite pipes and the major element compositional features of the lithospheric mantle have been reported elsewhere (Zhang et al. 1989; Dobbs et al. 1994; Wang et al. 1998a).

Mineral inclusions in diamonds from these two kimberlite pipes are almost exclusively of the peridotitic suite, with only a few of the eclogitic suite (Wang 1998). The full description of the studied samples is given in Table 1. They were selected from thousands of carats of industrial diamonds, and were free from any fractures under the optical microscope. About half of the studied diamonds contained only one single garnet inclusion, and the others had multiple grains of single-phase garnet or garnet coexisting with olivine or chromite. For example, four and three garnets were recovered from diamonds S03 and S06, respectively.

Two different techniques were used for removing mineral inclusions from the hosts, by mechanical cracking or by burning the host diamonds in air at ~800 °C for several hours. In the later case, diamonds were twice pre-cleaned before being placed into the furnace. This was necessary in order to avoid any possible contamination from impurities at the surfaces, which could sometimes be serious for trace elements. The burning technique allows one to extract all inclusions of various sizes from the diamond efficiently and safely without causing any alteration in the composition of silicate minerals (Taylor et al. 1996). It is especially useful when checking compositional similarities between multiple inclusions of one phase within a single diamond.

All recovered inclusions were encased in epoxy separately, and polished for analysis. Major element compositions were measured by the electron microprobe (JEOL JXA8800) at the Tokyo Institute of Technology. Natural silicate minerals and synthetic oxides were used as standards. All analyses were performed with accelerating voltage of 15 kV and focused electron beam with 12 nA current. Oxide ZAF corrections were applied. Sodium was usually analyzed first and counted for only 10 s without performing peak search, in order to minimize sodium evaporation. Counting times for other elements were 30–50 s. Concentrations of REE and some other trace elements were obtained using secondary ion microscopy (SIMS, Cameca IMS 3f) at the Tokyo Institute of Technology. A well-calibrated augite megacryst from alkali basalt of Japan and a quenched glass of JB-1 rock were used as standards. An energy filtering technique with an offset voltage of −40 V for REE and −100 V for other trace elements was applied to eliminate possible molecular interferences. The primary ion beam $^{16}O^-$ was about 20 μm in diameter. Analytical uncertainties originate mainly from counting statistics and are 10–20% for REE and 5–10% for other trace elements. Details about trace element measurement by SIMS have been presented separately (Yurimoto et al. 1989; Wang and Yurimoto 1994).

Phase chemistry

Major and trace element compositions of garnet inclusions in diamonds from the two kimberlite pipes are summarized in Tables 2 and 3. Compositions of some Cr-rich clinopyroxene inclusions, and of orthopyroxene and olivine inclusions from the same locality, were also analyzed. All studied samples are of ultramafic paragenesis. To illustrate major element characteristics of ultramafic garnets, the Cr_2O_3–CaO plot shown in Fig. 2 is frequently employed (Sobolev 1977). Garnets in the low-Ca area of this plot can be considered under-saturated in Ca, and probably were not in equilibrium with clinopyroxene. They are of harzburgitic paragenesis with compositions that indicate they might coexist only with orthopyroxene and olivine. Those in the high-Ca field probably equilibrated with clinopyroxene, even

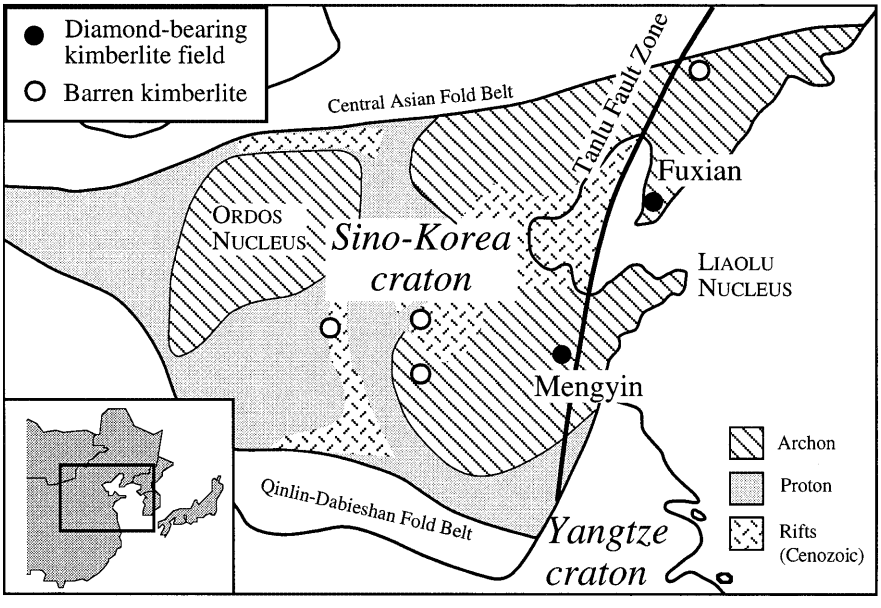

Fig. 1 Tectonic subdivisions of eastern China and occurrences of kimberlite fields (modified from Janse and Sheahan 1995). The Sino-Korea craton consists of two major nuclei, the Liaolu terrane in the east and the Ordos terrane in the west. The diamondiferous kimberlite fields locate in the opposing sides of the Tanlu Fault Zone. The Shengli 1 pipe is in the Mengyin kimberlite field, and the No.50 pipe is in the Fuxian field

Table 1 Description of the studied diamonds. *Py* Pyropic garnet, *ol* olivine, *sp* chromite, *n* a number of grains

Sample	Kimberlite pipe	Size (mm)	Shape	Color	Inclusions	Method[a]
L08	No.50	2.8	Octahedron	Colorless	1 py	Cracking
L09	No.50	3.0	Irregular	Colorless	1 py	Cracking
L10	No.50	2.0	Irregular	Colorless	1 py	Cracking
L11	No.50	2.5	Irregular	Colorless	1 py	Cracking
L12	No.50	1.8	Octahedron	Colorless	1 py	Cracking
L13	No.50	2.0	Irregular	Colorless	1 py	Cracking
L14	No.50	3.0	Irregular	Colorless	2 py	Cracking
L15	No.50	4.0	Flat chip	Colorless	1 py	Cracking
L16	No.50	4.2	Irregular	Colorless	1 py	Cracking
L22	No.50	2.0	Irregular	Colorless	1 py + 2 ol	Cracking
L23	No.50	2.0	Octahedron	Light brown	1 py + 1 ol	Cracking
L24	No.50	1.5	Octahedron	Colorless	1 py + 1 ol	Cracking
L25	No.50	1.2	Octahedron	Colorless	1 py	Cracking
S02	Shengli 1	2.0	Octahedron	Colorless	1 py	Burning
S03	Shengli 1	1.8	Octahedron	Colorless	1 py, n ol, 1sp	Burning
S04	Shengli 1	3.2	Octahedron	Colorless	4 py	Burning
S05	Shengli 1	2.2	Octahedron	Colorless	1 py, 1 ol	Burning
S06	Shengli 1	1.8	Octahedron	Colorless	3 py	Burning
S10	Shengli 1	3.5	{111}twin	Colorless	1 py, n ol	Burning
S24	Shengli 1	2.1	Oct. aggre.	Light yellow	1 py, n ol	Burning
S30	Shengli 1	2.0	Octahedron	Light yellow	1 py, n ol	Burning
Xiyu-1	Shengli 1	2.2	Irregular	Colorless	1 py	Cracking

[a] Techniques used for taking out mineral inclusions from diamonds

though it may not be present in the same diamond. Because Ca and Cr in garnet behave differently during partial melting of peridotite, Cr/Ca ratio is a good parameter showing how refractory is the peridotite in major element composition, although, as we discuss later, trace elements may behave differently from the major ones. The more refractory the peridotite, the higher the Cr/Ca ratio of garnet. The Cr/Ca ratio shows a positive correlation with its Mg/(Mg + Fe) for every individual pipe (Fig. 3).

Most of the studied garnet inclusions belong to the more refractory harzburgitic paragenesis. They are high in Cr_2O_3 (6–16 wt%) and relatively low in CaO, and exhibit a similar compositional range with that of the worldwide occurrences. Chondrite-normalized REE patterns (Anders and Grevesse 1989) of these harzburgitic garnets are shown in Fig. 4. Both the concentrations of REE and the patterns show extreme variation. With the exception of sample L15, which exhibited a nearly flat REE pattern, all the others displayed sinuous patterns. The abundance of light REE increases first from La to Pr, and then decreases from Sm to Dy. Concentrations of heavy REE are highly variable, showing a tendency to increase from Er to Lu in some samples. In the Shengli 1 kimberlite pipe, most garnet inclusions exhibit peaks at Nd_N (4.2–12.6). However, a large number of garnet inclusions from the No.50 pipe show peaks at Pr_N (5.3–60.7). Sample L25 is very rich in light REE, 10–15 times that of chondrite. From all 26 analyzed garnet inclusions, only one sample (S30-2) shows a Eu anomaly, with Eu/Eu* of about 2.7. Sinuous REE patterns, like those shown in Fig. 4, are a common feature for garnet inclusions in diamonds and harzburgitic garnet xenocrysts in kimberlites from Africa and Siberia (Nixon et al. 1987; Shimizu and Richardson 1987; Hoal et al. 1994; Shimizu et al. 1997a,b). However, a distinct positive Eu anomaly is very rare in peridotitic garnet. In comparison with other occurrences, some garnet inclusions from Chinese diamonds show relatively higher concentrations of light REE (Fig. 4).

Samples L10, L12, L24-1, and three garnets from the same diamond S06 are of lherzolitic paragenesis (Fig. 2). Sample L12 exhibits a typical "normal" REE pattern (Fig. 5). Light REE increase in abundance gradually from La to Sm (from 0.9 to 20.8), and the heavier elements from Sm to Lu remain flat or increase only slightly (20–28). Garnet L10 shows a similar normal REE pattern, with relatively higher concentrations in light REE and lower abundance in middle and heavy REE. In contrast, three garnets from diamond S06 show sinuous REE patterns, comparable to those of harzburgitic garnets. As a distinct feature, garnet L24-1 is very rich in both Cr_2O_3 (16.5 wt%) and CaO (9.2 wt%), with about 25 mol% of $Ca_3Cr_2Si_3O_{12}$. Because it plots in the elongated area of the lherzolitic field in Fig. 2, it is considered come from lherzolite. One olivine inclusion coexisted with garnet L24-1 in the same diamond host, but no unusual compositional features, at least in its major element composition (Fo, 92.5), were observed. Inclusion L24-1 is extremely rich in REE, the most among all studied garnet inclusions from China. It exhibits a sinuous REE pattern (Fig. 5), with light REE increasing from La_N of 27.1 to Pr_N of 60.7, then decreasing gradually from Nd to Lu, and having average heavy REE about ten times that of chondrite. Extremely high REE concentrations and the sinuous pattern of Cr_2O_3-rich lherzolitic garnet inclusions were also reported by Stachel and Harris (1997).

Garnet is a very common xenocryst in kimberlite and usually shows major element features similar to those

Table 2 Composition of garnet inclusions in diamonds from the Shengli 1 kimberlite pipe, China. Electron microprobe analyses as oxides in wt%, ion microprobe analyses as elements in wt ppm. *ND* Not detected

No.	S02	S03(2)	S04-2	S04-3	S04-4	S5(1)	S06-1	S06-2	S06-3	S10(1)	S24(1)	S30(2)-1	Xiyu-1
SiO_2	41.43	40.96	41.80	42.16	42.39	41.69	42.09	42.05	42.08	42.33	42.70	42.26	41.71
Al_2O_3	11.18	13.20	15.74	15.34	15.60	13.75	17.48	17.26	16.98	13.85	15.92	15.19	11.67
TiO_2	0.04	0.03	0.07	0.07	0.05	0.19	0.08	0.05	0.02	0.05	0.00	0.04	0.01
Cr_2O_3	15.35	12.74	9.49	10.30	10.83	11.88	7.82	8.42	8.35	12.27	9.57	8.92	14.13
FeO	6.85	6.61	6.70	7.10	6.96	7.00	6.15	6.57	6.54	5.08	5.91	5.81	6.45
NiO	0.04	0.00	0.00	0.00	0.08	0.00	0.02	0.03	0.02	0.04	0.00	0.02	0.00
MnO	0.50	0.45	0.42	0.49	0.41	0.44	0.39	0.44	0.36	0.29	0.31	0.28	0.39
MgO	20.69	18.56	19.58	19.97	20.59	20.26	19.20	18.59	19.42	24.26	24.04	22.73	21.99
CaO	4.52	6.82	5.49	5.42	5.40	4.78	6.65	6.41	6.71	1.70	1.73	3.35	3.23
Na_2O	0.03	0.01	0.00	0.00	0.00	0.02	0.04	0.02	0.00	0.02	0.00	0.03	0.00
K_2O	0.00	0.00	0.00	0.01	0.00	0.01	0.00	0.00	0.03	0.00	0.01	0.01	0.00
Total	100.63	99.38	99.29	100.85	102.31	100.02	99.92	99.84	100.50	99.88	100.20	98.64	99.57
Formula with oxygen number of 12													
Si	3.040	3.034	3.048	3.039	3.014	3.043	3.034	3.042	3.027	3.038	3.037	3.064	3.059
Al	0.966	1.152	1.353	1.304	1.307	1.183	1.485	1.472	1.440	1.171	1.334	1.298	1.009
Ti	0.002	0.002	0.004	0.004	0.003	0.011	0.005	0.003	0.001	0.002	0.000	0.002	0.000
Cr	0.890	0.746	0.547	0.587	0.609	0.685	0.446	0.481	0.475	0.696	0.538	0.511	0.819
Fe	0.420	0.410	0.408	0.428	0.414	0.427	0.371	0.397	0.393	0.305	0.352	0.352	0.395
Ni	0.003	0.000	0.000	0.000	0.005	0.000	0.001	0.002	0.001	0.002	0.000	0.001	0.000
Mn	0.031	0.028	0.026	0.030	0.025	0.027	0.024	0.027	0.022	0.017	0.018	0.017	0.024
Mg	2.320	2.101	2.183	2.201	2.238	2.260	2.116	2.056	2.136	2.661	2.614	2.520	2.465
Ca	0.355	0.541	0.429	0.418	0.411	0.373	0.513	0.496	0.517	0.131	0.132	0.261	0.254
Na	0.004	0.001	0.000	0.000	0.000	0.003	0.006	0.003	0.000	0.003	0.000	0.004	0.000
K	0.000	0.000	0.000	0.001	0.000	0.001	0.000	0.000	0.002	0.000	0.001	0.001	0.000
La	1.73	0.71	0.47	0.37	0.33	0.50	0.19	0.27	0.15	0.26	0.19	2.30	0.99
Ce	3.14	5.58	4.06	3.72	3.94	2.32	1.36	1.60	1.31	2.28	1.68	5.72	3.97
Pr	0.47	1.00	0.76	0.76	0.95	0.44	0.29	0.45	0.36	0.69	0.45	1.07	0.57
Nd	2.23	3.60	4.06	3.84	4.59	2.48	1.94	2.75	2.08	3.83	3.26	5.77	2.18
Sm	0.49	0.57	1.25	1.21	0.87	1.08	0.55	0.56	0.81	1.40	1.03	1.31	0.69
Eu	0.25	0.19	0.36	0.31	0.29	0.32	0.17	0.17	0.23	0.42	0.22	1.18	0.15
Dy	0.43	0.37	0.71	0.86	0.83	0.89	0.56	0.48	0.53	0.71	0.30	0.73	0.31
Ho	0.08	0.06	0.15	0.15	0.11	0.20	0.12	0.12	0.09	0.12	0.07	0.15	0.05
Er	0.26	0.24	0.39	0.40	0.31	0.47	0.24	0.28	0.25	0.41	0.21	0.34	0.15
Tm	0.03	0.04	0.08	0.05	0.04	0.08	0.04	0.04	0.04	0.04	0.06	0.06	ND
Yb	0.20	0.14	0.48	0.37	0.31	0.48	0.31	0.26	0.31	0.34	0.31	0.38	ND
Lu	0.02	0.05	0.06	0.04	0.07	0.10	0.07	0.04	0.05	0.05	0.02	0.05	0.02
Li	0.01	0.01	–	0.18	0.09	0.04	0.04	0.05	–	0.05	0.71	1.33	0.05
Na	41.1	21.0	–	71.2	69.8	81.4	38.7	40.4	–	25.3	31.0	52.2	53.2
K	7.82	1.76	–	5.27	1.83	1.37	5.14	10.46	–	1.57	14.62	193	3.50
Sc	338	468	–	331	342	285	208	210	–	255	200	189	294
Ti	672	59	–	517	527	1924	281	290	–	294	73	283	212
Sr	10.3	13.8	–	8.21	7.02	6.96	0.88	1.07	–	1.88	3.11	27.8	10.1
Y	1.51	1.12	–	2.79	3.01	4.61	1.95	1.80	–	2.39	0.19	1.63	0.59
Zr	9.44	7.59	–	12.1	14.8	25.3	11.8	12.2	–	15.7	0.18	14.0	4.90
Hf	0.59	0.00	–	0.64	2.29	1.29	0.53	0.00	–	0.78	0.54	0.43	0.20

occurring as inclusions in diamonds, but with a much wider compositional range. Figure 6 shows the REE patterns of some garnet xenocrysts from the Shengli 1 kimberlite pipe. Analogous to inclusions in diamonds, garnet xenocrysts in kimberlite of harzburgitic paragenesis show sinuous REE patterns, with similar enrichment in light REE. On the other hand, lherzolitic garnet xenocrysts always show the normal REE patterns; sinuous patterns have not been observed in this group. These lherzolitic garnet xenocrysts consistently have much higher heavy REE than do the inclusions.

Despite the very wide compositional ranges of garnet inclusions in diamonds for both major and rare earth elements, we were unable to find any evident correlation between them. For example, no definitive correlation can be detected from the summary plot of light REE against the Cr/Ca ratio (Fig. 7). Two pairs of garnet inclusions [L11 and L16; S5(1) and L25] have very similar major element compositions, both of which are of harzburgitic paragenesis. However, their REE patterns are entirely different (Fig. 8). For instance, light REE in sample L25 is about five to seven times higher than in S5(1), and in contrast middle and heavy REE are lower. From lherzolitic garnet inclusions, samples L10 and L12 have very similar major element compositions, but show distinctly different REE patterns, as depicted in Fig. 5. All these results indicate that the REE in garnet inclusions in diamonds from the two studied kimberlite pipes changed independently of their major element compositions.

Table 3 Composition of garnet inclusions in diamonds from the No.50 kimberlite pipe, China. Electron microprobe analyses as oxides in wt%, ion microprobe analyses as elements in wt ppm. NA Not analyzed; ND not detected

ppm Phase	L08 gt	L09 gt	L10 gt	L11 gt	L12 gt	L13 gt	L14-1 gt	L15 gt	L16 gt	L22-1 gt	L23-1 gt	L24-1 gt	L25 gt	L05 opx	L22-2 ol	L28 cpx	L31 cpx
SiO_2	42.44	42.95	42.42	41.31	42.11	41.02	43.45	41.50	41.69	40.38	41.56	39.46	39.41	58.53	41.33	55.66	55.61
Al_2O_3	14.76	18.82	17.69	13.50	17.92	15.53	18.48	17.20	13.33	14.01	16.76	10.54	14.07	0.60	0.00	1.02	0.75
TiO_2	0.02	0.00	0.03	0.10	0.16	0.03	0.01	0.02	0.02	0.04	0.03	0.15	0.07	0.00	0.00	0.03	0.00
Cr_2O_3	11.30	5.96	6.73	13.25	6.56	10.50	6.63	8.66	12.85	13.28	8.90	16.52	11.6	0.37	0.08	1.22	1.07
FeO	5.83	5.63	6.37	6.03	5.80	6.27	5.23	5.90	6.63	5.54	5.73	5.36	5.97	4.42	6.13	2.00	2.34
NiO	0.03	0.00	0.04	0.01	0.02	0.00	0.01	0.02	0.03	0.04	0.03	0.00	0.03	0.11	0.36	0.02	0.06
MnO	0.33	0.27	0.33	0.38	0.31	0.37	0.29	0.30	0.40	0.30	0.30	0.34	0.33	0.13	0.12	0.12	0.06
MgO	22.75	23.94	20.37	20.67	21.03	20.97	23.74	21.97	19.43	23.72	22.63	17.62	21.66	35.58	51.35	18.74	18.61
CaO	2.35	1.66	5.77	5.64	5.94	4.78	2.91	4.90	5.39	3.40	4.46	9.17	4.92	0.88	0.03	20.28	20.73
Na_2O	0.01	0.00	0.01	0.02	0.04	0.01	0.01	0.02	0.03	0.04	0.02	0.00	0.01	0.06	0.00	0.97	0.70
K_2O	0.01	0.01	0.01	0.00	0.00	0.01	0.00	0.01	0.00	0.01	0.01	0.01	0.01	0.01	0.01	0.18	0.22
Total	99.8	99.23	99.77	100.91	99.89	99.5	100.76	100.5	99.79	100.75	100.41	99.18	98.08	100.69	99.38	100.23	100.13
Oxygen no.	12	12	12	12	12	12	12	12	12	12	12	12	12	6	4	6	6
Si	3.051	3.040	3.046	2.997	3.015	2.988	3.040	2.968	3.057	2.915	2.972	2.980	2.933	1.975	0.991	1.990	1.994
Al	1.251	1.570	1.497	1.154	1.512	1.333	1.524	1.450	1.152	1.192	1.412	0.938	1.234	0.024	0.000	0.043	0.032
Ti	0.001	0.000	0.002	0.005	0.009	0.002	0.001	0.001	0.001	0.002	0.002	0.009	0.004	0.000	0.000	0.001	0.000
Cr	0.642	0.333	0.382	0.760	0.371	0.605	0.367	0.490	0.745	0.758	0.503	0.986	0.683	0.010	0.001	0.034	0.030
Fe	0.351	0.333	0.383	0.366	0.347	0.382	0.306	0.353	0.407	0.335	0.343	0.338	0.372	0.125	0.123	0.060	0.070
Ni	0.002	0.000	0.002	0.001	0.001	0.000	0.001	0.001	0.002	0.002	0.002	0.000	0.002	0.003	0.007	0.001	0.002
Mn	0.020	0.016	0.020	0.023	0.019	0.023	0.017	0.018	0.025	0.018	0.018	0.022	0.021	0.004	0.002	0.004	0.002
Mg	2.501	2.590	2.236	2.293	2.302	2.335	2.539	2.402	2.178	2.618	2.474	2.034	2.464	1.835	1.883	1.024	1.020
Ca	0.181	0.126	0.444	0.438	0.456	0.373	0.218	0.376	0.424	0.263	0.342	0.742	0.392	0.032	0.001	0.777	0.796
Na	0.001	0.000	0.001	0.003	0.006	0.001	0.001	0.003	0.004	0.006	0.003	0.000	0.001	0.004	0.000	0.067	0.048
K	0.001	0.001	0.001	0.000	0.000	0.001	0.000	0.001	0.000	0.001	0.001	0.001	0.001	0.000	0.000	0.008	0.010
La	0.90	0.22	0.46	0.40	0.21	0.15	0.34	0.20	0.94	0.83	0.61	6.40	3.32	ND	ND	NA	NA
Ce	5.38	2.70	2.44	3.83	1.82	2.03	3.74	0.89	6.95	7.41	5.23	37.07	10.52	ND	ND	NA	NA
Pr	0.98	0.60	0.49	0.89	0.60	0.66	0.84	0.16	1.35	1.27	0.95	5.64	1.23	ND	ND	NA	NA
Nd	5.01	3.31	3.20	4.38	4.59	3.55	4.18	0.96	5.62	5.07	3.31	20.64	3.63	ND	ND	NA	NA
Sm	1.29	0.11	1.29	0.97	3.10	0.58	0.29	0.27	1.22	1.50	0.30	2.93	0.53	ND	ND	NA	NA
Eu	0.32	0.03	0.33	0.23	1.20	0.10	0.08	0.08	0.28	0.42	0.04	0.86	0.13	ND	ND	NA	NA
Dy	0.37	0.10	1.54	0.92	6.92	0.16	0.29	0.20	0.41	0.89	0.16	2.74	0.33	ND	ND	NA	NA
Ho	0.08	0.03	0.27	0.14	1.37	0.03	0.08	0.05	0.06	0.15	0.04	0.54	0.07	ND	ND	NA	NA
Er	0.26	0.08	0.89	0.48	4.07	0.20	0.22	0.18	0.19	0.49	0.12	1.75	0.25	ND	ND	NA	NA
Tm	0.05	0.02	0.11	0.09	0.52	0.02	0.03	0.03	0.03	0.07	0.04	0.23	0.05	ND	ND	NA	NA
Yb	0.32	0.31	1.00	0.42	3.84	0.23	0.24	0.26	0.26	0.51	0.32	1.61	0.47	ND	ND	NA	NA
Lu	0.06	0.06	0.16	0.09	0.55	0.04	0.06	0.04	0.03	0.07	0.05	0.22	0.07	ND	ND	NA	NA
Li	0.04	0.06	0.08	1.87	0.26	1.02	1.73	0.08	0.02	0.03	0.03	0.04	0.02	0.50	0.99	0.43	1.11
Na	19.6	15.5	67.3	157.5	128.5	24.6	55.2	70.8	19.4	35.9	32.1	75.1	29.6	210	53.6	5942	4148
K	0.75	1.91	13.8	6.65	4.66	1.26	10.2	3.53	0.45	3.69	0.70	5.76	1.34	22.33	0.78	1314	1739
Sc	303	203	227	185	192	201	142	169	352	472	242	321	284	3.07	1.8	21.5	10.0
Ti	198	24.8	256	658	1487	87.7	46.5	229	117	445	264	1322	613	27.2	4.5	348	303
Sr	9.67	5.54	2.25	3.46	2.75	1.71	6.19	1.59	9.02	12.4	4.75	37.8	19.3	1.00	0.38	438	372
Y	1.83	0.26	10.30	3.67	48.30	0.43	1.11	1.25	1.11	4.12	0.92	16.7	2.21	0.02	0.01	2.17	1.32
Zr	5.80	0.70	42.9	9.23	151	2.27	2.43	1.40	5.09	15.20	3.08	36.0	6.66	0.12	0.14	2.24	0.69
Hf	0.74	1.40	1.19	0.22	18.0	0.08	0.09	1.33	0.25	2.57	0.62	9.27	1.38	0.29	1.06	0.45	0.95

Two diamonds contained multiple garnet inclusions. Three garnet inclusions from each diamond S04 and S06 were large enough for trace element analysis. In terms of major element composition, some relatively small variations can be seen among inclusions from the same diamond host, especially in the Cr_2O_3 contents of those from diamond S04. In spite of that, we can regard these inclusions from the same diamond host as having similar major element compositions. The REE patterns of six garnets from the two separate diamond hosts are displayed in Fig. 9. In contrast to the report by Shimizu and Sobolev (1995), we failed to find any evident variations of REE between the multiple grains of garnet from the same host, within the analytical uncertainties of the trace elements. Grain sizes of all garnet inclusions in this study were less than 100 μm, with most within 30–80 μm. While the detailed mapping of trace element distribution within a single garnet, like that performed by Shimizu and Sobolev (1995), could not be carried out in this study due to their relatively smaller grain sizes, two to three randomly selected points on single grains of a large number of garnet inclusions from the No.50 pipe were analyzed by ion microprobe. The analysis failed to detect any significant compositional variations within single garnet grains. In a brief summary valid for the garnet inclusions from the two Chinese kimberlite pipes,

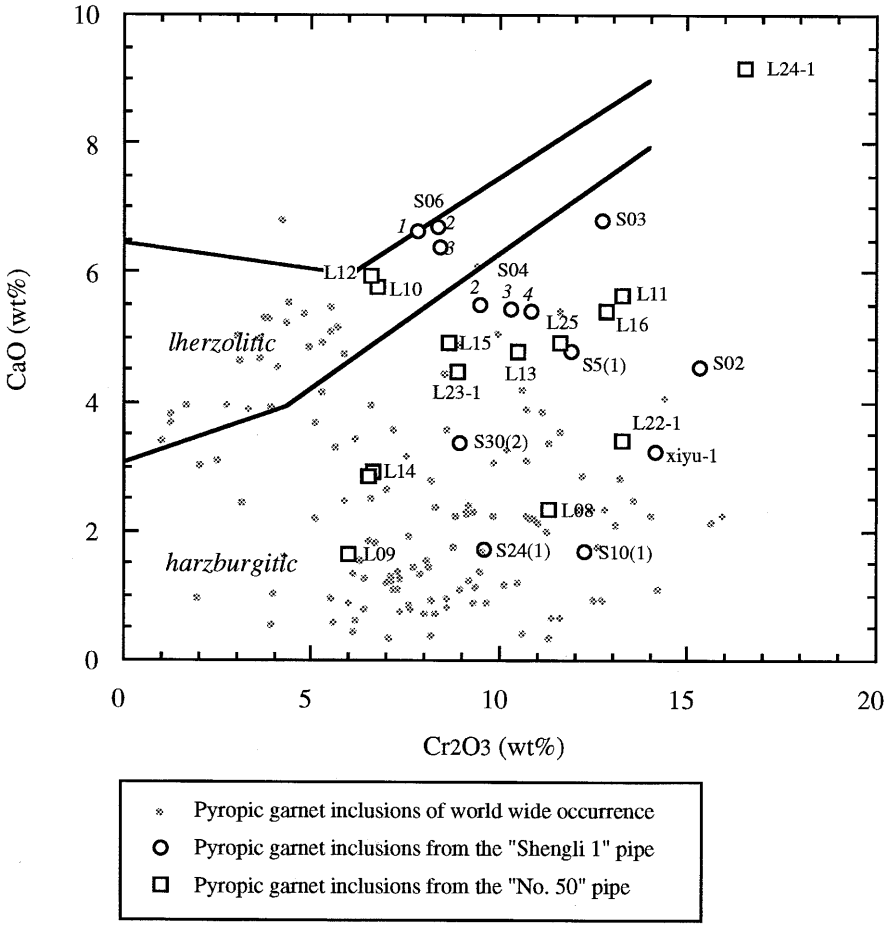

Fig. 2 The $CaO–Cr_2O_3$ plot for garnet inclusions in diamonds from two Chinese kimberlite pipes. Most garnets are of harzburgitic parageneses, and a few are of calcium saturated lherzolitic parageneses. The boundaries separating the two parageneses are from Sobolev (1977). Compositions of peridotitic garnet inclusions in diamonds from other worldwide occurrences are shown for comparison

while substantial differences in REE exist among the inclusions from separate diamond hosts, those from the same host are basically identical and homogeneous.

Concentrations of trace elements Na, Ti, Zr, Li, and Sr in garnet inclusions are plotted in Fig. 10 as a function of their Cr/Ca ratio. For comparison, those of garnet xenocrysts from the two kimberlite pipes are also shown. All these trace elements are incompatible in garnet, and should decrease gradually with increasing degree of partial melting. Consistent correlation with Cr/Ca is observed for Na, Ti, and Zr, as expected, and their concentrations decrease gradually as the Cr/Ca ratio increases. Sodium contents in the most fertile garnets reach 600 ppm, and decrease to about only 10 ppm in the most refractory garnets. However, Sr and Li show much more complex relations. Lherzolitic garnet inclusions are obviously much lower in the concentration of these two elements, in comparison with the more refractory harzburgitic garnet inclusions. Contents of Li in lherzolitic garnet inclusions are less than 0.4 ppm, and Sr of less than 4 ppm; in contrast, Li and Sr in harzburgitic garnet inclusions may reach as high as 2 ppm and 40 ppm, respectively. Considering the difference in mineral assemblages, lherzolitic garnet is saturated with Ca and should coexist with diopsidic clinopyroxene in addition to olivine and orthopyroxene.

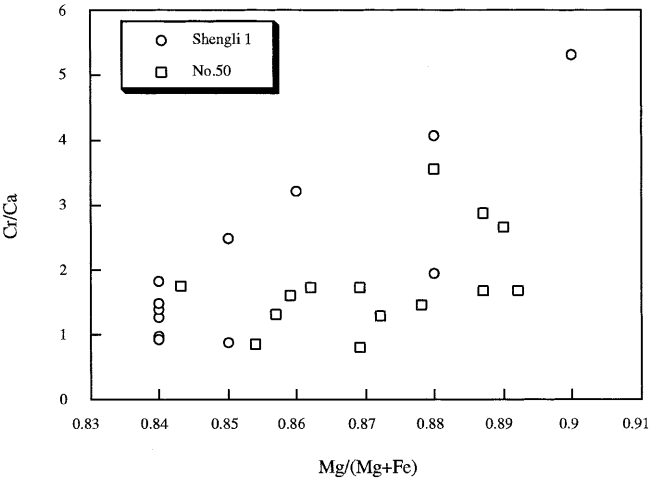

Fig. 3 Variation of the atomic ratio of Mg/(Mg + Fe) as a function of Cr/Ca of garnet inclusions in Chinese diamonds. A positive correlation is evident between the two ratios

As shown in Table 3, Sr is strongly partitioned into clinopyroxene (372–438 ppm), which is the main reservoir of Sr instead of garnet (Stachel and Harris 1997). In the absence of clinopyroxene in harzburgite, garnet contains most of Sr. Among the harzburgitic garnet

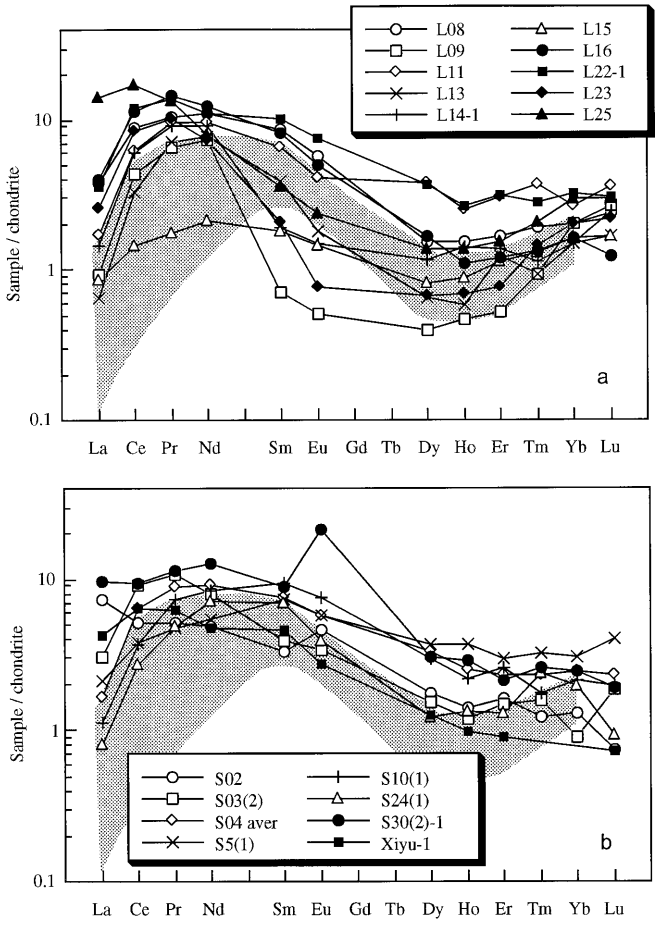

Fig. 4 Chondrite normalized REE patterns of harzburgitic garnet inclusions in diamonds from the No.50 kimberlite pipe **a**, and the Shengli 1 kimberlite pipe **b**. In contrast to their extremely refractory major element compositions, these garnets are enriched in more incompatible light REE, but in a kind of downward-concave pattern. Concentrations of REE vary greatly and are different from diamond to diamond. *Shaded region* shows most peridotitic garnet inclusions from African and Siberian diamonds (Shimizu and Sobolev 1995; Shimizu et al. 1997a)

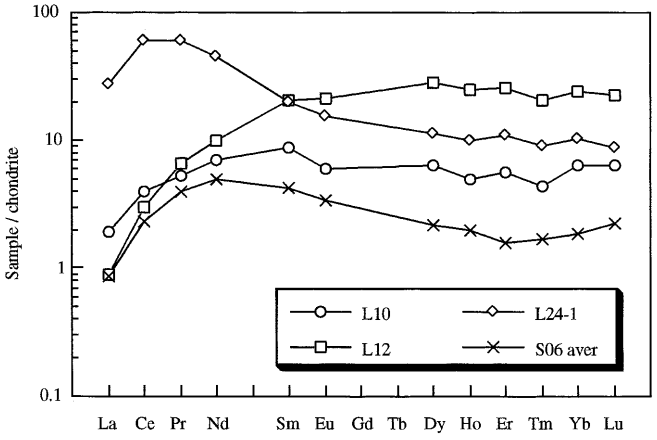

Fig. 5 Chondrite-normalized REE patterns of lherzolitic garnet inclusions from diamonds. Both normal and sinuous patterns exist, and sample L24-1 is extremely rich in REE. S06 is the average value of three garnet inclusions in one diamond from the Shengli 1 pipe, and the other three samples are from the No.50 pipe

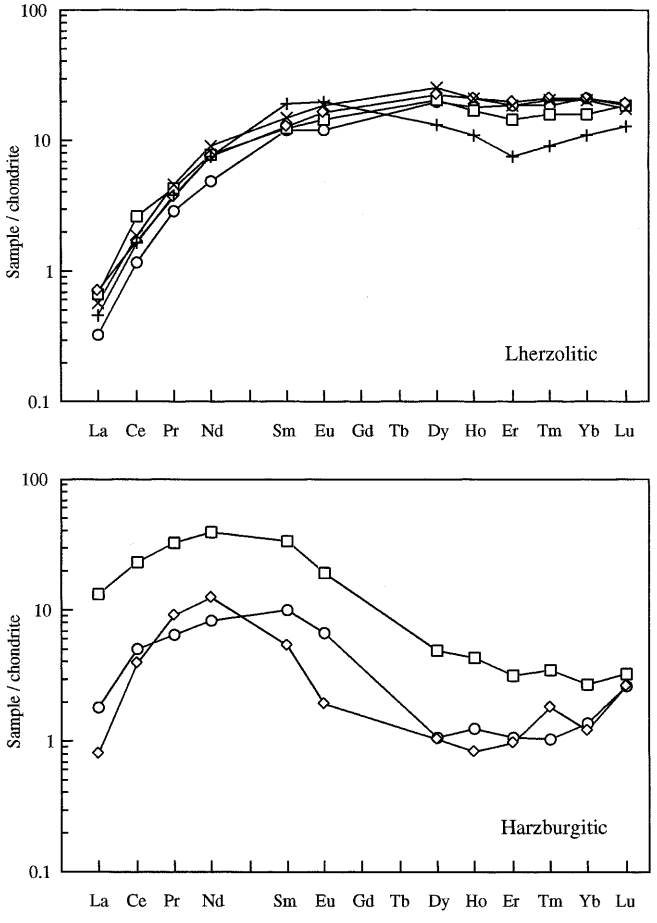

Fig. 6 Chondrite-normalized REE patterns of garnet xenocrysts from the Shengli 1 kimberlite pipe. Unlike those from inclusions in diamonds, no sinuous patterns were observed from lherzolitic garnet xenocryst

inclusions, contents of Li and Sr decrease gradually as they become more refractory (higher Cr/Ca ratio). In comparison, garnet xenocrysts in kimberlites, regardless of the lherzolitic or harzburgitic paragenesis, have very low contents of Li and Sr. For Sr, all xenocrysts are below 5 ppm, with only one exception reaching 20 ppm. Evident differences between the harzburgitic garnet inclusions in diamonds and those of the same paragenesis occurring as xenocrysts in kimberlites apparently link the formation of diamond to some additional processes responsible for those differences.

Discussion

Enrichment of the Archean lithospheric mantle

The extremely refractory nature of the Archean lithospheric mantle in major element composition is well documented (Boyd 1989; Boyd et al. 1997). The similarity of the lithospheric mantle beneath the Sino-Korea craton to other cratonic areas has also been recognized

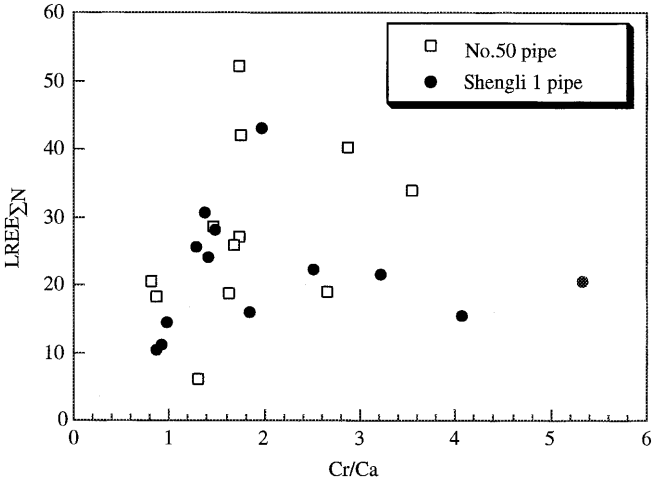

Fig. 7 Variation in total light REE (chondrite normalized) of garnet inclusions in diamonds as a function of their Cr/Ca ratio. No specific correlation is evident, indicating that REE concentrations in garnet inclusions vary independently of their major element compositions

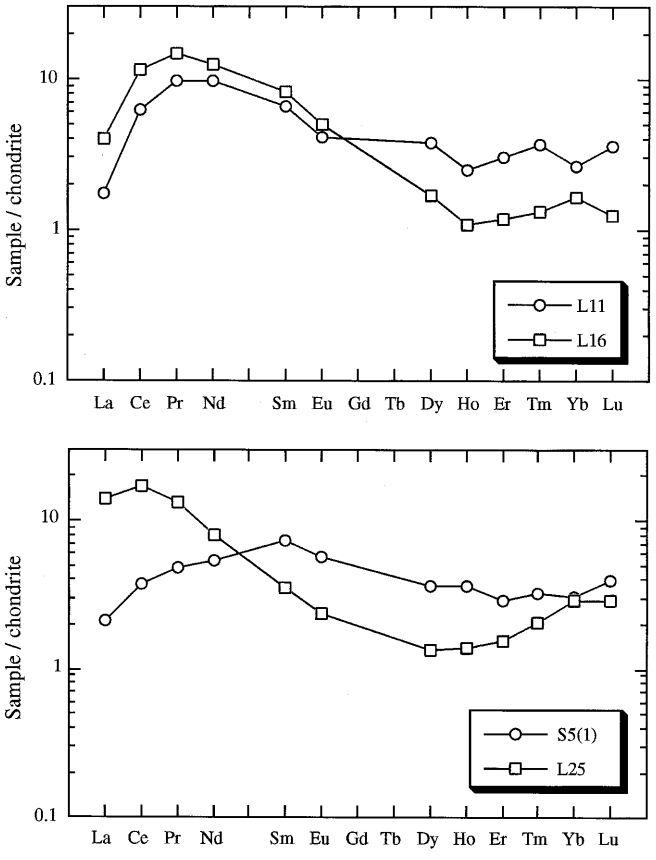

Fig. 8 Chondrite-normalized REE patterns of two pairs of garnet inclusions in diamonds, which have very similar major element compositions but completely different trace element compositions

(Wang et al. 1998a), including the high Mg/(Mg + Fe) and Cr/Ca ratios of the studied mineral inclusions from diamonds. Large degrees partial melting and melt extraction from fertile peridotites may lead to

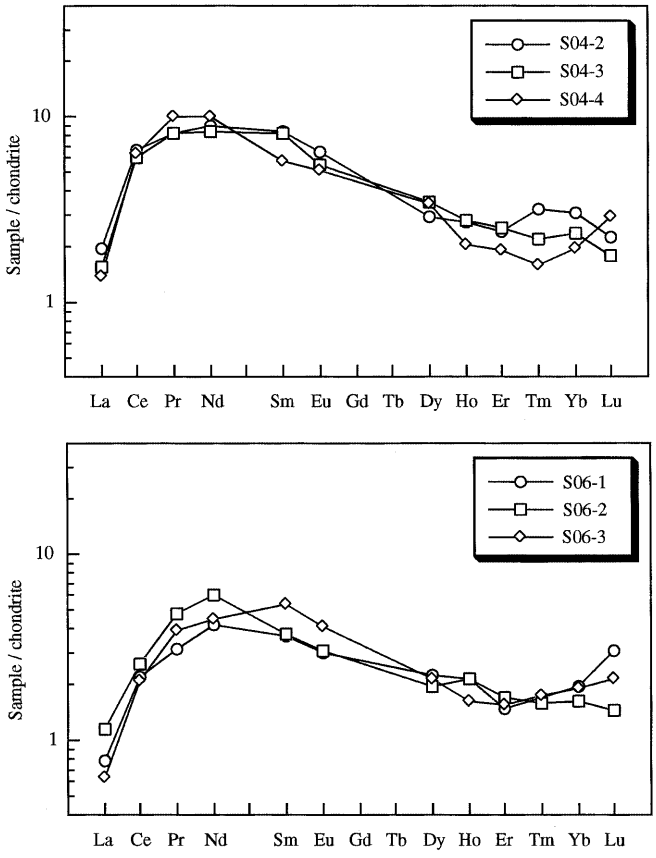

Fig. 9 Chondrite-normalized REE patterns of multiple garnet inclusions from a single diamond host. No evident variations were observed within the analytical uncertainties. Both diamonds S04 and S06 are from the Shengli 1 kimberlite pipe

the formation of such refractory peridotites as residues (Jordan 1978; Boyd 1989; Walker et al. 1989; Takahashi 1990; Walter 1998). The observed enrichment of light REE and other very incompatible trace elements in the harzburgitic garnets is obviously in direct conflict with their major element composition, and hence cannot be explained by single or multiple stage partial melting and melt extraction. Late one-stage or multistage enrichment processes, such as interactions with metasomatic melts very rich in incompatible elements, appear unavoidable.

Harzburgitic garnets, no matter whether occurring as inclusions in diamonds or xenocrysts in kimberlites, exhibit sinuous REE patterns. Concentrations of REE and other trace elements like Ti, Sr, Zr, and Li change significantly from grain to grain, and cover a very large compositional range. High field strength elements (HFSE), like Zr and Ti, are relatively depleted in harzburgitic garnet inclusions. All these features are also observed in garnet inclusions from Africa and Siberia (Nixon et al. 1987; Shimizu and Richardson 1987; Hoal et al. 1994; Stachel and Harris 1997; Griffin et al. 1999), and very possibly are common and global features for all other Archean lithospheric mantle, instead of being a local phenomenon varying with occurrence. This sug-

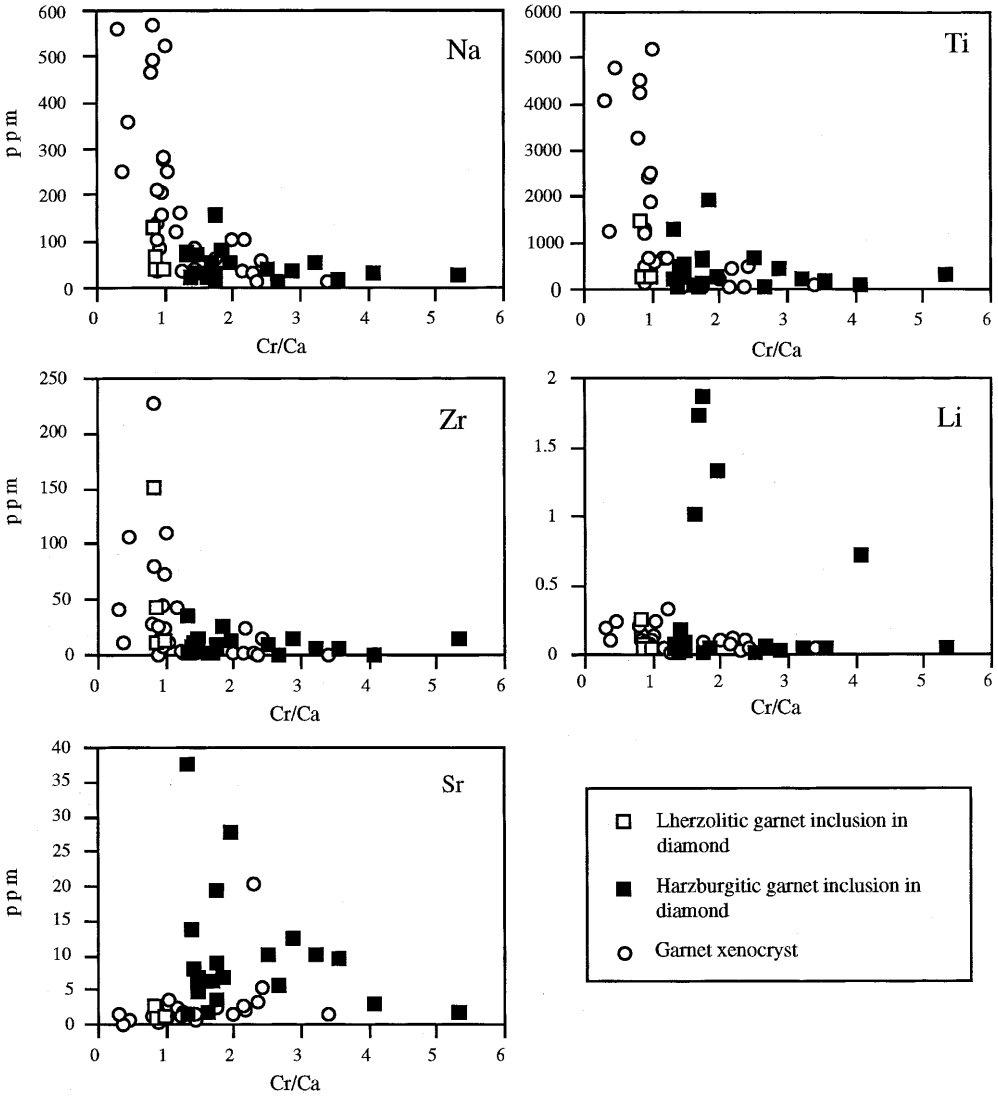

Fig. 10 There are consistent correlation between major and trace element compositions of garnet inclusions in diamonds, but those of harzburgitic garnet inclusions show much more complex variations (see text for more explanation). With the increasing Cr/Ca ratio, concentrations of these incompatible elements in garnet decrease consistently. Analytical data for garnet xenocrysts from the same two kimberlite pipes are shown for comparison

gests that a similar metasomatic process is responsible for all these enrichments taking place beneath the Archean cratons. Since the metasomatic melt is likely to be of carbonatite composition, as we discuss in the next section, we suspect that this enrichment process is not related to melts from subducted oceanic crust. While the carbonatite metasomatism seems to be most common in the continental Archean lithospheric mantle possibly due to its ancient age, it also occurs in other tectonic areas (Green and Wallace 1988; Yaxley et al. 1991; Dautria et al. 1992; Rudnick et al. 1993; Blusztajn and Shimizu 1994; Shimizu and Sobolev 1995; Shimizu et al. 1997a, b; Yaxley et al. 1998), even in the oceanic upper mantle (Coltorti, et al. 1999) and hotspot-related region (Hauri et al. 1993). This suggests strongly that the carbonatite metasomatism occur worldwide, but at varying depths depending on the tectonic settings.

Relatively higher mode of enstatite, and thus low Mg/Si ratio (average 1.22), is an important feature of granular peridotite xenoliths from Kaapvaal craton, southern Africa (Boyd 1989). Kimberlites in the Sino-Korea craton contain few mantle xenoliths. Extensive study of the mineral inclusions in Chinese diamonds and the preliminary study of mantle xenoliths showed that the enstatite modes of peridotite from the Sino-Korea craton were not so high as those from Kaapvaal, in spite of it being similarly Mg-rich (Wang et al. 1998a). The estimated Mg/Si ratio is about 1.26–1.31. Similar observations were also reported from the Siberia cratonic peridotites (Pearson et al. 1995a). Hence, the low Mg/Si ratio is not a common feature for all Archean cratonic peridotites. Herzberg (1993) pointed out that peridotite of low Mg/Si ratio could not form as residues by partial melting of fertile peridotite. Alternatively, it was proposed that the excess enstatite was secondary, formed by interaction of depleted peridotite with SiO_2-rich melts generated mainly by partial melting of eclogitic basalt and sediment in a subduction zone (Kelemen et al. 1998). Carbonatite melt poor in SiO_2 may not contribute much to the formation of excess enstatite. It is very

possible that infiltration of both SiO_2-rich and carbonatite melts happened in the ancient continental lithosphere, but with variable intensities among different cratons. The Sino-Korea craton experienced relatively weak SiO_2-rich infiltration, but more extensive carbonatite melt metasomatism, as revealed in its relatively high Mg/Si ratio of peridotite and high concentrations of light REE in garnet inclusions of diamonds (Fig. 4).

Models for the metasomatism

Properties of metasomatic melts and details about metasomatic reactions are far from clear and different models were proposed to explain these enrichment processes. Hoal et al. (1994) adopted a disequilibrium metasomatic model to explain the REE patterns of mantle peridotitic garnets, in which REE diffused into an existing garnet with a normally light REE depleted pattern and very low overall REE content. They proposed that both the "normal" and "sinusoidal" REE patterns of peridotitic garnets are the products of metasomatism of previously existing mantle garnets by some kind of light REE-enriched melts or fluids, but only the lherzolitic garnets with the normal REE patterns have achieved equilibrium with the metasomatic melts or fluids. They insisted that the development of the sinuous REE patterns of the harzburgitic garnets were due to the sluggishness of the heavy REE diffusion in garnet, when compared with light REE during the re-equilibration process. The following observations in this study, however, are inconsistent with this model:

1. Some extremely incompatible trace elements, for example, Sr, Nb, Li, and K, are much more abundant in some harzburgitic garnets (with the sinuous REE pattern) than in the less refractory lherzolitic garnets (with the normal REE pattern) (Fig. 10; Tables 2, 3). If only the lherzolitic garnets achieved equilibrium with metasomatic melts, it can be expected that the abundance of these elements in lherzolitic garnets would be much higher.
2. Lherzolitic garnet inclusion L24-1 contains the most abundant amount of REE in garnet among the studied garnets. Instead of having a normal REE pattern, it is strongly enriched in light REE. Its $(Ce/Yb)_N$ value is as high as 6.0.
3. Within the analyzed samples, some harzburgitic garnets are more enriched in light REE than the lherzolitic ones (Figs. 4 and 5). This implies that even the light REE in the lherzolitic garnets, which have the normal REE patterns, would not have achieved equilibrium with metasomatic melts, assuming that the metasomatic model of Hoal et al. (1994) is correct.
4. Diffusion rates of REE in garnet have not been yet experimentally determined. In contrast to Hoal et al.'s expectation, diffusion rates of heavy REE in garnet could be faster than those of light REE, considering the relatively smaller ion radii of heavy REE.
5. There is no definitive evidence that the peridotitic garnets with the normal REE patterns have been metasomatized. In the laboratory, garnet generated by single or multistage melting of fertile peridotite is expected to have a normal REE pattern, but evidently it experienced no metasomatism at all.

In contrast to the disequilibrium models, Griffin et al. (1999) recently pointed out that the trace element characteristics of harzburgitic garnet could be explained by an equilibrium relation with carbonatite melts. According to their explanation, the low heavy REE and the enrichment in the middle REE reflect the steep chondrite-normalized REE patterns of carbonatite melts, while the low light REE in those garnets reflect the progressive misfit of the larger REE in the garnet structure, especially in the absence of the large Ca ion for which they can substitute. Due to the special physical and chemical properties of carbonatite melts, the chemical interaction of mantle peridotite with CO_2-rich melts has often been invoked in order to explain the trace element enrichment in alkali magmas and included mantle peridotite xenoliths. Actually, some mantle xenoliths occurring in alkali basalts could also be explained reasonably as the result of this reaction, and thus in support of the existence of Ca-rich carbonatite metasomatic melt in the mantle (Green and Wallace 1988; Yaxley et al. 1991, 1998; Dautria et al. 1992; Hauri et al. 1993; Rudnick et al. 1993; Blusztajn and Shimizu 1994; Coltorti et al. 1999). Carbonatite melts are very low in viscosity and hence able to percolate easily through olivine-rich mantle rocks (Hunter and MacKenzie 1989; Watson et al. 1990). Additionally, new experiments have shown that the melting temperature of a CO_2-rich primitive kimberlite is rather low (1350–1450 °C) at 5–23 GPa (Wang and Gasparik, unpublished). Such a low liquidus temperature of CO_2-rich melt indicates that carbonatite melts can easily be generated in the deep mantle. Interaction of Ca-rich carbonatite melt with mantle peridotite could lead to the precipitation of secondary clinopyroxene and olivine by the reaction of the carbonatite melt with orthopyroxene. This should increase the Ca/Al, Zr/Hf ratios and light REE contents of peridotite, but without affecting its Mg/(Mg + Fe). Relatively low concentrations of HFSE are another important feature of carbonatite melts (Nelson et al. 1988).

Concerning the bulk trace element concentrations in harzburgite, the REE contents in olivine and orthopyroxene occurring as inclusions in diamonds are very low, below the detection limits of SIMS. Contents of HFSE like Ti and Zr are a factor of ten lower than those in garnets (Tables 2 and 3). The bulk composition of harzburgite basically mimics that of garnet, being relatively rich in light REE but poor in HFSE (Fig. 11). In general, signatures of enrichment in REE without concomitant enrichment in HFSE (Ti, Zr, Hf) in mantle-derived peridotite, as well as those in harzburgitic garnet xenocrysts and inclusions in diamonds, are consistent

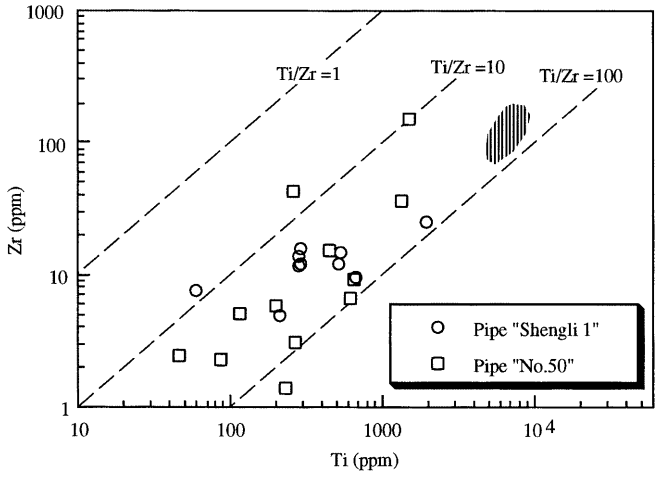

Fig. 11 Plot of the concentrations of Zr vs. Ti in garnet inclusions from diamonds, showing that the concentrations of HFSE Zr and Ti in garnet inclusions are lower than in garnets from fertile lherzolites (*shaded area*) reported by Shimizu and Richardson (1987)

with the chemical interaction involving carbonatite melts. Shimizu and Richardson (1987), Shimizu and Sobolev (1995), and Stachel and Harris (1997) argued against a simple equilibrium relationship between garnet and metasomatic melt, because the hypothetical melts are much more fractionated in REE composition than kimberlitic, lamproitic, or carbonatitic melts. No melt with such a fractionated REE composition has ever been observed. Additionally, the equilibrium model cannot easily explain the following observations of this study:

1. The downward-concave light REE patterns in almost all of the harzburgitic garnets, with peak shifting between Pr and Nd. This is not in agreement with the REE patterns of carbonatite melts, in which no evident concave pattern in light REE has been observed. In contrast to silicate melt (e.g., Shimizu and Kushiro 1975; Wang et al. 1998b), little information is available for REE partitioning between garnet and carbonatite melt, but the possibility of a sudden and progressive decrease in the partitioning coefficients is unlikely.

2. Equilibrium between garnet and Ca-rich carbonatite melt may lead to the formation of Ca-rich garnet, contrary to the observed subcalcic compositions. The partitioning coefficient for Ca between garnet and carbonatite melt under the conditions corresponding to the bottom of the lithospheric mantle is 0.4–0.5 (Wang and Gasparik, unpublished). Contents of CaO in most carbonatite melts reaching the earth's surface are higher than 15 wt%, with an average of 36 wt% (Nelson et al. 1988). Assuming a similar composition for the carbonatite metasomatic melt, the CaO content of garnet in equilibrium with the melt should be much higher than those observed in inclusions from diamonds. In addition to the Ca-rich carbonatite melts, Rudnick et al. (1993) pointed out that the metasomatic carbonatite melt could also be Mg-rich, based on their research on xenoliths from northern Tanzania. Even so, it seems to be unrealistic to expect that all metasomatic carbonatite melts in the lithospheric mantle are Mg-rich, and only those reaching the surface are Ca-rich.

3. As a distinct feature, the Zr/Hf ratio of carbonatite melts is very high. According to the data reported by Nelson et al. (1988), the average value of Zr/Hf of carbonatite melts is about 1280, which is much larger than the chondritic value of 39. No evident increase of the Zr/Hf ratio was detected in the garnet inclusions studied here. However, the analysis of Hf in this study may suffer from larger uncertainties than for other elements owing to its low concentrations, but this should not have a major effect on the range of Zr/Hf. The Zr/Hf ratios of most garnet inclusions are within 21–42, with an average value of 30. If an equilibrium relationship with the carbonatite metasomatic melt were achieved, this ratio in garnet should be much higher.

4. Extremely large variations in trace element contents of garnet inclusions even from the same locality, as shown in Figs. 4 and 5, and especially of those garnets with very similar major element compositions but completely different REE patterns, cannot be fully explained as the result of equilibrium metasomatism by one or more carbonatite melts.

The ratio of melt to rock fundamentally controls the metasomatic mechanism and processes (Rudnick et al. 1993). The local spatial orientation of any veins will contribute significantly to the variation of this ratio in space. Depending on this ratio, metasomatism may happen in two different forms. If this ratio is high enough, the metasomatism is accomplished in an open system. In this case, given enough reaction time, equilibrium between the crystal and melt could be achieved, and thus the composition of the metasomatic melts can be quantified using proper partition coefficients of trace elements. On the contrary, with a low ratio of melt to rock, the metasomatism will be accomplished in a "closed or freezing" system. The metasomatic melt is frozen in the mantle rocks, and progresses in the form of bulk mixing of the metasomatic melt and mantle rock. When a limited amount of carbonatite melt intrudes into a patch of lithospheric mantle, even considering its high mobility in peridotite, a significant gradient in the ratio of melt to rock may develop. Intrusion of carbonatitic melt into the relatively low-temperature lithospheric mantle could possibly lead to partial melting of peridotite. In such a case, it acts just like the open-system melting models proposed by Dick et al. (1984) and Ozawa and Shimizu (1995), which involve continuous influx of light REE-enriched melt into mantle peridotite, inducing melting and melt extraction from the melting region as melting proceeds. Analogous to the gradient in the ratio of melt to rock, a gradient in temperature may also exist, resulting in variable degree of partial melting. Additionally, several episodes of intrusions of carbonatite melts with different compositions could be involved in metasomatic reactions.

Based on the previous discussions, we believe that the trace element features observed from the garnet inclusions in Chinese diamonds are mainly caused by carbonatite melt infiltration and partial melt extraction. Spatial and temporal gradients in melt/rock ratio and temperature are the main reasons for the large variations of REE patterns and other trace element concentrations. Most of the individual diamonds, in contrast, may crystallize under relatively stable kinetic conditions.

Compositional heterogeneities of inclusions in diamonds

Heterogeneous trace element distribution within single garnet inclusions and significant variations among multiple garnet inclusions from the same diamond host, as reported by Shimizu and Sobolev (1995) from Siberian diamonds, were interpreted to suggest that these diamonds formed shortly before the eruption of kimberlite at 360 Ma ago. Otherwise, the observed heterogeneities within single garnet inclusions would have been wiped out by diffusion. On the other hand, radioactive isotope analysis revealed much older model (3.0–3.5 Ga) and isochron age (1.9 Ga) of peridotitic diamonds (Richardson et al. 1984, 1993). Detailed mapping of trace element distribution could not be performed in the present study, but analyses of randomly selected two to three points on a large number of garnet inclusions from the No.50 diamonds showed no apparent chemical variation. Multiple grains of one phase from single diamonds, for example the three garnets recovered from diamond S04 and another three from diamond S06, exhibit very similar trace element compositions. These results indicate that trace element heterogeneity within individual inclusions or between multiple inclusions from the same diamond host is not a common feature for the Chinese diamonds, in spite of significant variations in both major and trace element compositions among diamonds from the same locality.

It is usually assumed that a mineral inclusion in diamond is completely isolated from its surroundings by the host diamond, and no chemical exchange has occurred after its capture, if there are no cracks around the inclusion or annealing features observed under optical microscope (e.g., Wang 1998). This assumption may not be always correct. Figure 12 shows the remains of a diamond after burning at 800 °C for 8 h in air. This diamond is from the Shengli 1 pipe, and no cracks were observed under the optical microscope. Garnet inclusions are connected and supported by two crosscutting films, which are colorless and extremely thin. Attempts to analyze the composition of these films by EDS failed due to quick evaporation even under a weak scanning electron beam. These films are secondary, formed by filling cracks in diamonds. Through these thin films, chemical exchange between the inclusions and the surroundings can easily happen, especially when evident changes in pressure and temperature are involved. In this case, the two garnet inclusions had severely altered rims. The thinner the film is, the more difficult it is to observe it even by the burning technique. It is not necessary that the observed chemical heterogeneities of the mineral inclusions in Siberian diamonds were caused by the same mechanism, because similar films were not reported (Shimizu and Sobolev 1995; Shimizu et al. 1997a). Additionally, this process is difficult to explain the extremely high contents of Sr (500–2000 ppm) at rims of garnet inclusions from Siberian diamonds. However, effort should be made to identify these microfractures in diamonds, when noticing chemical heterogeneities in their mineral inclusions.

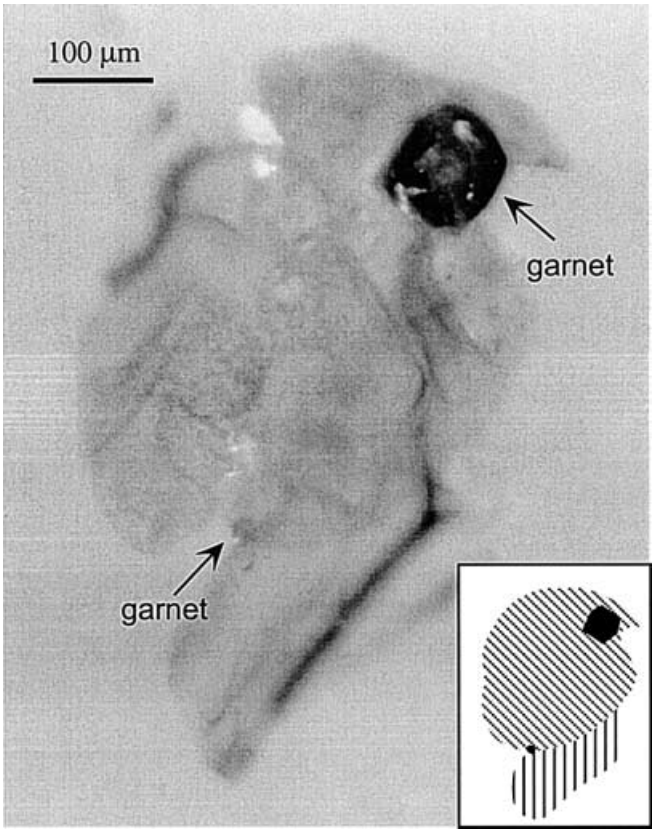

Fig. 12 Remains of a diamond from the Shengli 1 kimberlite pipe, after burning at 800 °C for about 8 h in air. The diamond was of irregular and rounded shape, and no cracks could be observed under optical microscope. Two eclogitic garnet inclusions are connected and supported by two crosscutting colorless thin films. Rims of the two inclusions show evident alteration as the result of chemical exchange with the surroundings through the thin films (micro-cracks)

Acknowledgments N. Shimizu and S.B. Shirey are thanked for their constructive reviews, which improved this paper significantly. We are indebted to X. Wang, Q. Miao, and Q. Yang, of the Bureau of Geology and Mineral Resources of Liaoning province, P.R. China, for assistance in the field trip and sample collection. This work was supported by the Monbusho scholarship, the Research Fellowship of the Japan Society for the Promotion of Science for Young Scientists (P97053), and by the National Science Foundation grant EAR-9710158. This is Mineral Physics Institute publication 253 at the Department of Geosciences, SUNY, Stony Brook.

References

Anders E, Grevesse N (1989) Abundances of the elements – meteoritic and solar. Geochim Cosmochim Acta 53: 197–214

Blusztajn J, Shimizu N (1994) The trace-element variations in clinopyroxenes from spinel peridotite xenoliths from southwest Poland. Chem Geol 111: 227–243

Boyd FR (1989) Compositional distinction between oceanic and cratonic lithosphere. Earth Planet Sci Lett 96: 15–26

Boyd FR, Pokhilenko NP, Pearson DG, Mertzman SA, Sobolev NV, Finger LW (1997) Composition of the Siberian cratonic mantle: evidence from Udachnaya peridotite xenoliths. Contrib Mineral Petrol 128: 228–246

Coltorti M, Bonadiman C, Hinton RW, Siena F, Upton BGJ (1999) Carbonatite metasomatism of the oceanic upper mantle: evidence from clinopyroxenes and glasses in ultramafic xenoliths of Grande Comore, Indian Ocean. J Petrol 40: 133–165

Dautria JM, Dupuy C, Yakherist D, Dostal J (1992) Carbonate metasomatism in the lithospheric mantle: peridotitic xenoliths from a melilititic district of the Sahara basin. Contrib Mineral Petrol 111: 37–52

Dick HJB, Fisher RL, Bryan WB (1984) Mineralogical variability of the uppermost mantle along mid-ocean ridges. Earth Planet Sci Lett 69: 88–106

Dobbs PN, Duncan DJ, Hu S, Shee SR, Colgan EA, Brown MA, Smith CB, Allsopp HL (1994) The geology of Mengyin kimberlites, Shandong, China. In: Meyer HOA, Leonardos OH (eds) Kimberlites, related rocks and mantle xenoliths. CPRM Spec Publ 1A/93, pp 40–61

Green DH, Wallace ME (1988) Mantle metasomatism by ephemeral carbonatite melts. Nature 336: 459–462

Griffin WL, Shee SR, Ryan CG, Win TT, Wyatt BA (1999) Harzburgite to lherzolite and back again: metasomatic processes in ultramafic xenoliths from the Wesselton kimberlite, Kimberley, South Africa. Contrib Mineral Petrol 134: 232–250

Hauri EH, Shimizu N, Dieu JJ, Hart SR (1993) Evidence for hotspot-related carbonatite metasomatism in the oceanic upper mantle. Nature 365: 221–227

Herzberg CT (1993) Lithosphere peridotites of the Kaapvaal craton. Earth Planet Sci Lett 120: 13–29

Hoal KEO, Hoal BG, Erlank AJ, Shimizu N (1994) Metasomatism of the mantle lithosphere recorded by rare earth elements in garnets. Earth Planet Sci Lett 126: 303–313

Hunter RH, MacKenzie D (1989) The equilibrium geometry of carbonate melts in rocks of mantle composition. Earth Planet Sci Lett 92: 347–356

Jahn BM, Auvray B, Cornichet J, Bai YL, Shen QH, Liu DY (1987) 3.5 Ga old amphibolites from eastern Hebei province, China: field occurrence, petrography, Sm–Nd isochron age and REE geochemistry. Precambrian Res 34: 311–346

Janse AJA, Sheahan PA (1995) Catalogue of worldwide diamond and kimberlite occurrences: a selective and annotative approach. J Geochem Explor 53: 73–112

Jordan TH (1978) Composition and development of the continental tectosphere. Nature 274: 544–548

Kelemen PB, Hart SR, Bernstein S (1998) Silica enrichment in the continental upper mantle via melt/rock reaction. Earth Planet Sci Lett 164: 387–406

Liu DY, Nutman AP, Compston W, Wu JS, Shen QH (1992) Remnants of 3800 Ma crust in the Chinese part of the Sino-Korea craton. Geology 20: 339–342

Nelson DR, Chivas AR, Chappell BW, McCulloch MT (1988) Geochemical and isotopic systematics in carbonatites and implications for the evolution of ocean-island sources. Geochim Cosmochim Acta 52: 1–17

Nixon PH, van Calsteren PWC, Boyd FR, Hawkesworth CJ (1987) Harzburgites with garnets of diamond facies from Southern African kimberlites. In: Nixon PH (ed) Mantle xenoliths. Wiley, Chichester, pp 523–533

Ozawa K, Shimizu N (1995) Open-system melting in the upper mantle: constraints from the Hayachine–Miyamori ophiolite, northeastern Japan. J Geophys Res 100: 22315–22335

Pearson DG, Shirey SB, Carlson WR, Boyd FR, Pokhilenko NP, Shimizu N (1995a) Re–Os, Sm–Nd, and Re–Sr isotope evidence for thick Archean lithospheric mantle beneath the Siberian craton modified by multistage metasomatism. Geochim Cosmochim Acta 59: 959–977

Pearson DG, Carlson RW, Shirey SB, Boyd FR, Nixon PH (1995b) Stabilization of Archean lithospheric mantle: a Re–Os isotopic study of peridotite xenoliths from the Kaapvaal craton. Earth Planet Sci Lett 134: 341–357

Richardson SH, Gurney JJ, Erlank AJ, Harris JW (1984) Origin of diamonds in old enriched mantle. Nature 310: 198–202

Richardson SH, Harris JW, Gurney JJ (1993) Three generations of diamonds from old continental mantle. Nature 366: 256–258

Rudnick RL, McDonough WF, Chappell BW (1993) Carbonatite metasomatism in the northern Tanzanian mantle: petrography and geochemical characteristics. Earth Planet Sci Lett 114: 463–475

Shimizu N, Kushiro I (1975) The partitioning of rare earth elements between garnet and liquid at high pressure: preliminary experiments. Geophys Res Lett 2: 413–416

Shimizu N, Richardson SH (1987) Trace element abundance patterns of garnet inclusions in peridotite-suite diamonds. Geochim Cosmochim Acta 51: 755–758

Shimizu N, Sobolev NV (1995) Young peridotitic diamonds from the Mir kimberlite pipe. Nature 375: 394–397

Shimizu N, Sobolev NV, Yefimova ES (1997a) Chemical heterogeneities of inclusion garnets and juvenile character of peridotitic diamonds from Siberia. Russ Geol Geophys 38: 356–372

Shimizu N, Pokhilenko NP, Boyd FR, Pearson DG (1997b) Geochemical characteristics of mantle xenoliths from the Udachnaya kimberlite pipe. Russ Geol Geophys 38: 205–217

Sobolev NV (1977) Deep-seated inclusions in kimberlites and the problem of the composition of the upper mantle. Am Geophys Union, Washington, DC

Stachel T, Harris JW (1997) Diamond precipitation and mantle metasomatism – evidence from the trace element chemistry of silicate inclusions in diamonds from Akwatia, Ghana. Contrib Mineral Petrol 129: 143–154

Takahashi E (1990) Speculations on the Archean mantle: missing link between komatiite and depleted garnet peridotite. J Geophys Res 95: 15941–15954

Taylor LA, Snyder GA, Crozaz G, Sobolev VN, Yefimova ES, Sobolev NV (1996) Eclogitic inclusions in diamonds: evidence of complex mantle processes over time. Earth Planet Sci Lett 142: 535–551

Walker RJ, Carlson RW, Shirey SB, Boyd FR (1989) Os, Sr, Nd and Pb isotope systematics of southern Africa peridotite xenoliths: implication for the chemical evolution of subcontinental mantle. Geochim Cosmochim Acta 53: 1583–1595

Walter MJ (1998) Melting of garnet peridotite and the origin of komatiite and depleted lithosphere. J Petrol 39: 29–60

Wang W (1998) Formation of diamond with mineral inclusions of "mixed" eclogite and peridotite paragenesis. Earth Planet Sci Lett 160: 831–843

Wang W, Yurimoto H (1994) Analysis of rare earth elements in garnet by SIMS. Annu Rep, Inst Geosci, Univ Tsukuba 19: 87–91

Wang W, Takahashi E, Sueno S (1998a) Geochemical properties of lithospheric mantle beneath Sino-Korea craton; evidence from garnet xenocrysts and diamond inclusions. Phys Earth Planet Inter 107: 249–260

Wang W, Sueno S, Takahashi E (1998b) Influence of Cr on REE partitioning between garnet and silicate melt: application to metasomatism of mineral inclusions in diamonds. Rev High Press Sci Technol 7: 92–94

Watson EB, Brennan JM, Baker DR (1990) Distribution of fluids in the continental mantle. In: Menzies MA (ed) Continental lithosphere. Clarendon Press, Oxford, pp 111–125

Yaxley GM, Crawford AJ, Green DH (1991) Evidence for carbonatite metasomatism in spinel peridotite xenoliths from western Victoria, Australia. Earth Planet Sci Lett 107: 305–317

Yaxley GM, Green DH, Kamenetsky V (1998) Carbonatite metasomatism in the southern Australian lithosphere. J Petrol 39: 1917–1930

Yurimoto H, Yamashita A, Nishida N, Sueno S (1989) Quantitative SIMS analysis of GSJ rock reference samples. Geochem J 23: 215–236

Zhang P, Hu S, Wan G (1989) A review of the geology of some kimberlites in China. In: Ross J (ed) Kimberlites and related rocks, vol 1, their composition, occurrence, origin and emplacement. Geol Soc Aust, pp 329–400